Research Article

Ranjan K. Mohapatra*, V. P. Saikishore, Mohammad Azam*, Susanta K. Biswal*

Synthesis and physicochemical studies of a series of mixedligand transition metal complexes and their molecular docking investigations against Coronavirus main protease

https://doi.org/10.1515/chem-2020-0190 received August 29, 2020; accepted November 28, 2020

Abstract: A novel series of mixed-ligand complexes of the type, $[M(L_1)(L_2)Cl] \cdot 2H_2O$ $[L_1 = 2-(\alpha-methyl salicylidene$ hydrazine) benzimidazole (primary ligand), $L_2 = 2,2'$ bipyridine (bipy; secondary ligand), M = Co(II), Ni(II), Cu(II) and Zn(II), were based on the physicoanalytical studies. The spectroscopic findings revealed tridentate nature of the Schiff base ligand (L₁) and its coordination to the metal ions via azomethine nitrogen, ring nitrogen and the deprotonated phenolic oxygen atoms. Furthermore, the synthesized compounds were evaluated for antimicrobial activity against Bacillus subtilis, Escherichia coli and Salmonella typhi microorganisms. In addition, molecular docking studies were carried out against Middle East respiratory syndrome coronavirus (PDB ID: 4ZS6) and severe acute respiratory syndrome coronavirus 2 main protease (PDB ID: 6W63).

Keywords: Schiff base, ternary complexes, spectral, antimicrobial, molecular docking studies

1 Introduction

Benzimidazole, an important precursor of the heterocyclic compounds, exhibits a wide range of biological

applications, i.e., antiviral, antifungal, antipyretic, antidepressant and inhibitory activities in various cancers [1–5]. The broad biological activity of these compounds is supposed to be due to the presence of sp² hybridized nitrogen donor atoms [6]. The ligational behavior of benzimidazole and its derivatives has been explored in coordination chemistry to form stable complexes through various modes of coordination [7]. The benzimadazolebased metal complexes exhibit broad spectrum of pharmaceutical activities, such as zinc complexes of benzimidazole find usage in anticancer activity, and reveal remarkable antimicrobial activity [8]. In addition, several benzimadazole complexes have been reported as anticancer agents [9,10]. It is also reported that the transition metal ions form stable complexes and have displayed several properties [11,12]. Over the years, bipy and its derivatives have received immense importance as binding blocks and ligands in the construction of various homo- and heteroleptic metal complexes with broad spectrum of applications in the area of both material and biological science [13-17].

Mixed-ligand complexes, which have two different ligands, find significant consideration in coordination chemistry because of their structural variation and diverse applications [18,19]. Besides, mixed-ligand complexes also exhibit various biological applications [20]. Recent outbreak due to severe acute respiratory syndrome coronavirus 2 (SARS-CoV-2) has destroyed the economy and various socioeconomic sectors worldwide [21–23]. So far, not a single approved drug is available to treat the caused infection. Therefore, scientists are trying to find a drug to combat the COVID-19 pandemic. Several reports suggest that the progression of this pandemic can be controlled by targeting the main protease (M^{pro}) to develop the potential inhibitor. Molecular docking, a computational strategy to predict the binding site to assist drug repositioning for several diseases, plays a significant role in the pharmaceutical industry to bring new drugs to the market [24]. The HIV-1 protease inhibitors as the repurposed drugs for SARS-CoV-2 M^{pro} are discussed in literature [24–26]. Therefore, considering the versatile nature of mixed-ligand complexes, we are reporting four

^{*} Corresponding author: Ranjan K. Mohapatra, Department of Chemistry, Government College of Engineering, Keonjhar, Odisha, India, e-mail: ranjank_mohapatra@yahoo.com, mhashim@ksu.edu.sa

^{*} Corresponding author: Mohammad Azam, Department of Chemistry, College of Science, King Saud University, Riyadh PO BOX 2455, Riyadh 11451, Saudi Arabia, e-mail: azam_res@yahoo.com

^{*} Corresponding author: Susanta K. Biswal, Department of Chemistry, Centurion University of Technology and Management, Odisha, India, e-mail: dr.skbiswal@cutm.ac.in

V. P. Saikishore: Department of Chemistry, Centurion University of Technology and Management, Odisha, India

new mixed-ligand complexes of Co(II), Ni(II), Cu(II) and Zn(II) ions with benzimidazole-based Schiff base ligand (L_1) as the primary ligand, and bipy as the co-ligand, (L_2) in 1:1:1 molar ratio, and investigated them by various physicochemical studies. The synthesized metal complexes exhibited moderate antibacterial activity when screened against *Bacillus subtilis*, *Escherichia coli* and *Salmonella typhi*. In addition, we analyzed the molecular docking of the complexes of protein obtained from Middle East respiratory syndrome coronavirus (MERS-CoV; PDB ID: 4ZS6) and SARS-CoV-2 M^{PO} (PDB ID: 6W63).

2 Experimental

2.1 Preparation of the benzimidazole derived Schiff base ligand, L₁

The precursor, 2-hydrazinobenzimidazole, was prepared following the previously reported protocol [27]. The primary ligand, L₁, was prepared by the condensation reaction of 2-hydrazinobenzimidazole with *o*-hydroxyacetophenone in equimolar ratio in ethanol [27].

Yield 80%, color yellow; anal. calc. (%): C, 63.83; H, 4.96; N, 19.86, found (%): C, 63.76; H, 4.92; N, 19.82.

2.2 Preparation of mixed-ligand complexes

An ethanolic solution of the Schiff base ligand, L_1 (0.01 mol and 20 mL), metal(II) chloride (0.01 mol and 20 mL) and bipy, and L_2 (0.01 mol and 20 mL) were mixed in 1:1:1 molar ratio and refluxed for 2.5 h at pH = 7–8 by

adding catalytic amount of solid NaOH. A colored precipitate was obtained, which was separated by filtration. The precipitate was washed with methanol and dried in vacuo. The schematic representation of the synthesis of mixed-ligand complexes is given in Scheme 1.

2.3 In vitro antibacterial activity

The *in vitro* antimicrobial activity of the studied mixed-ligand complexes was reported by Agar Well diffusion method [27] at $100 \,\mu g \, mL^{-1}$ concentrations against *B. subtilis, E. coli* and *S. typhi* with ciprofloxacin as the standard antibacterial drug.

2.4 Molecular docking study

In order to evaluate the biological activity, molecular docking was analyzed on CLC Drug Discovery Workbench Software to obtain accurate predictions about the structure and interactions with a protein/enzyme receptor [28]. Some protein/enzyme receptors were imported from protein data bank (http://www.rcsb.org/:PDB): MERS-CoV (PDB ID: 4ZS6 [29]) and SARS-CoV-2 M^{pro} (PDB ID: 6W63 [30]).

In the docking simulation, the compounds (Figure 1) were placed into a predictable binding site on the surface of a protein target. The CLC Drug Discovery Work bench utilized MMFF94 (Merck Molecular Force Field [MMFF]) force field to generate 3D structure on import. Rotation around bond generates several conformations. Thus, the ligand optimizer was realized by geometry minimization using MMFF94 force field [31], conforming the binding

Scheme 1: Schematic representation of preparation of mixed-ligand complexes.

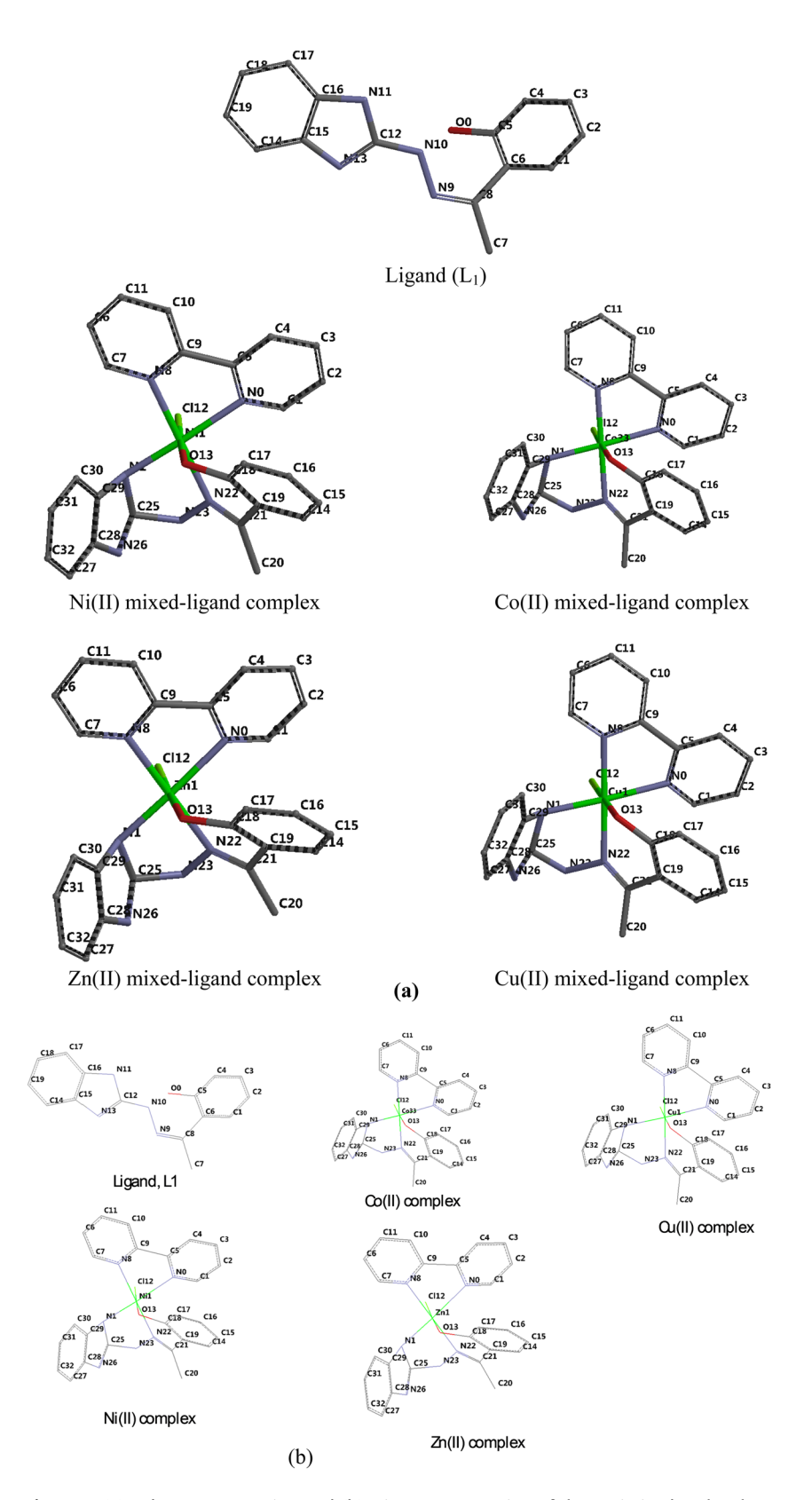


Figure 1: (a) Tube representation and (b) wire representation of the optimized molecular structure of ligand and mixed-ligand metal complexes (numbering of the atoms was done according to the software).

pocket geometry. The protein-ligand interaction was scored, and the best score-binding mode was returned for individual ligand and collected with the score. The ligand-binding mode search is effectuated inside the binding site (green sphere with a radius large enough to comprise the ligands docked to the receptor protein). After the import of the protein receptor from the PDB bank, the next step involved the setting up of the binding site and the binding pockets; binding pockets are necessary to guide the docking simulation. After the setup of the binding site and the binding pocket, the co-crystallized-natural ligand was extracted and redocked in the active binding site of the protein receptor to validate the method and the docking parameters obtained from the molecular docking studies.

Ethics approval: The conducted research is not related to either human or animal use.

3 Results and discussion

All the synthesized mixed-ligand complexes are stable at room temperature, non-hygroscopic and soluble in dimethyl sulfoxide and *N,N*-dimethylformamide. The physicoanalytical data are shown in Table 1.

3.1 Fourier-transform-infrared (FT-IR) spectra

The FT-IR spectra revealed the coordination of the metal ion through the deprotonated phenolic oxygen atom by the disappearance of the band at \sim 3,300 cm⁻¹ due to the phenolic –OH stretching vibration [32,33]. This was further confirmed by the hypsochromic shift of phenolic $v_{\rm (C-O)}$ band at \sim 1,280 cm⁻¹ in the free ligand and L_1 to \sim 1,500 cm⁻¹ in the spectra of the mixed-ligand complexes [33,34]. However, the position of the band due to $v_{\rm N-H}$

(exocyclic) remains practically unaltered in the spectra, suggesting its noninvolvement in coordination [33] (Figure S1). Furthermore, noncoordination of ring nitrogen atom $v_{(-C=N)}$ of benzimidazole moiety in the spectra of the complexes is also ascertained by finding no change in the positions of the characteristic IR bands at ~1,540 and ~1,320 cm $^{-1}$ due to $v_{(C=N)}$ (cyclic) and $v_{(C-N)}$ (cyclic) modes of vibration, respectively [33]. On the other hand, the position due to benzimidazole $v_{(N-H)}$ at ~3,150 cm⁻¹ reduced to lower frequency of ca. 20-25 cm⁻¹, suggesting participation of -NH group of benzimidazole in coordination [33,35]. However, the bands due to $v_{(C=N)}$ and $v_{(N-N)}$ vibrations also show negative shift of ca. 10-20 cm⁻¹ in the spectra of the complexes, suggesting their role in coordination [33,36]. Moreover, the vibration at \sim 3,450 cm⁻¹ is assigned to $v_{\rm (O-H)}$ of the lattice water [33,34]. In addition, a sharp band at 655–680 cm⁻¹ due to $v_{(C=N)}$ of pyridine is observed in the spectra of the complexes [33,37].

3.2 Electronic spectra

The electronic spectral data and the magnetic moment values of the mixed-ligand complexes are listed in Table S1. The electronic spectrum of Co(II) complex showed two main bands at $\sim 10,745 \,\mathrm{cm}^{-1}$ (broad) and $\sim 22,136 \,\mathrm{cm}^{-1}$ (strong) due to ${}^4T_{1g}(F) \rightarrow {}^4T_{2g}(F)$ (v_1) and ${}^4T_{1g}(F) \rightarrow {}^4T_{1g}$ (P) (ν_3) transitions, respectively [38,39]. However, ${}^4T_{1g}(F)$ \rightarrow ⁴A_{2g}(F) (ν_2) transition was not observed because of its association with a large amount of energy cause by two electron transitions ($t_{2g}^5 e_g^2 \rightarrow t_{2g}^3 e_g^4$) [39,40]. Furthermore, the observed magnetic moment, $\mu_{\rm eff}$ (4.72 BM), supported an octahedral geometry around Co(II) ion [39,41]. The studied mixed-ligand complex of Ni(II) complex showed split bands at ~8,850 and ~ 10,420 cm⁻¹ assigned to ${}^{3}B_{1g} \rightarrow {}^{3}E_{g}$ and ${}^{3}B_{1g} \rightarrow {}^{3}B_{2g}$ transitions, respectively. In addition, two characteristic bands at ~15,350 and ~24,575 cm⁻¹ were assigned to ${}^3A_{2g}(F) \rightarrow {}^3T_{1g}(F)$ (ν_2) and ${}^3A_{2g}(F) \rightarrow {}^3T_{1g}(P)$ (v_3) transitions, respectively, and suggested an octahedral

Table 1: Physicoanalytical data of the compounds

Sl. no.	Compounds	Molecular mass	Yield (%)	Λ_{m}^{a}	C found (calcd)	H found (calcd)	N found (calcd)	M found (calcd)
1	[CoL ₁ L ₂ Cl]2H ₂ O	533.5	66	14.5	53.92 (53.98)	4.08 (4.12)	15.69 (15.74)	11.01 (11.06)
2	$[NiL_1L_2Cl]2H_2O$	538	71	11.3	53.69 (53.53)	4.02 (4.09)	15.55 (15.61)	11.75 (11.80)
3	$[CuL_1L_2Cl]2H_2O$	533	68	12.7	53.96 (54.03)	4.07 (4.12)	15.71 (15.76)	10.93 (10.97)
4	$[ZnL_1L_2Cl]2H_2O$	539.5	65	9.2	53.32 (53.38)	4.03 (4.07)	15.50 (15.57)	11.98 (12.04)

a Ohm⁻¹ cm² mole⁻¹.

Table 2: TGA data for the ternary compounds

Compounds	Temp. range of	% of water loss		Decomposition	% of residue		Composition
	water loss (°C)	Found	Calc.	temperature (°C)	Found	Calc.	of the residue
[CoL ₁ L ₂ Cl]2H ₂ O	60-110	6.69	6.74	270	14.01	14.05	CoO
[NiL ₁ L ₂ Cl] 2H ₂ O	55-110	6.70	6.75	260	13.92	13.98	NiO
$[CuL_1L_2Cl]2H_2O$	45-95	6.65	6.69	255	14.72	14.77	CuO
$[ZnL_1L_2Cl]2H_2O$	50-100	6.62	6.67	240	14.93	15.01	ZnO

geometry around Ni(II) ion, which was confirmed by the observation of magnetic moment at 2.98 BM [39,42]. The mixed-ligand complex of Cu(II) displayed two bands at ~14,320 and ~16,775 cm $^{-1}$ attributed to $^2B_{1g} \rightarrow ^2B_{2g}$ (ν_2) and $^2B_{1g} \rightarrow ^2E_g$ (ν_3) transitions, respectively, thus suggesting a distorted octahedral geometry [39,43]. However, the band due to $^2B_{1g} \rightarrow ^2A_{1g}$ was not observed in the studied copper complex [39,44]. The μ_{eff} value for copper complex at 1.88 BM also suggested an octahedral geometry [39,45].

3.3 Thermal analysis

The thermogravimetric analysis (TGA) data for the studied mixed-ligand complexes displayed similar pattern of thermal decomposition. The lattice water degraded at temperature below 100°C in all the studied complexes. This is followed by the degradation of the anhydrous complexes in two distinct stages at temperatures 250–280°C and 360–390°C. However, the degradation of organic constituents continued until the formation of stable metal oxide as the end product. The temperature ranges of decomposition, peak temperature and the possible fragments removed are presented in (Table 2).

3.3.1 Proton nuclear magnetic resonance (¹H-NMR) spectra

The $^1\text{H-NMR}$ spectra of Schiff base ligand, L_1 , and its mixed-ligand complex of Zn(ii) displayed a multiplet due to the aromatic protons at δ 7.3–8.1 ppm. The signals at δ 6.7 and δ 9.0 ppm were attributed to the ring NH and exocyclic NH protons, respectively (Figure S2). However, the observed de-shielding in the ring –NH proton at δ 7.0 ppm indicated its participation in coordination. Furthermore, disappearance of phenolic –OH proton in the metal complexes confirmed its role in coordination. Moreover, –CH $_3$ signal was also observed at δ 2.4 ppm.

3.4 Antibacterial activity

The in vitro antibacterial activity was reported by Agar well diffusion method [27] against B. subtilis, E. coli and S. tvphi at 100 µg mL⁻¹ concentrations. The zone of inhibition data was studied using ciprofloxacin as the standard antibacterial drug as shown in Figure 2. The studied complexes exhibited better activity than the free ligand, which is likely due to the presence of -C=N linkage and its involvement in coordination. Furthermore, coordination through the metal ions reduces the electron density due to the partial sharing of its positive charge with the donor groups and possible π -electron delocalization [46]. In addition, solubility, dipole moment, the nature of the ligand and geometry are supposed to be the possible factor for the higher antibacterial activity displayed by the mixed-ligand complexes [47]. However, the mixedligand Zn(II) complex remained inactive against E. coli and S. typhi.

3.4.1 Docking evaluation against MERS-CoV

Docking studies were performed to obtain accurate predictions on the optimized conformations for both the ligands and protein target to form a stable complex. All

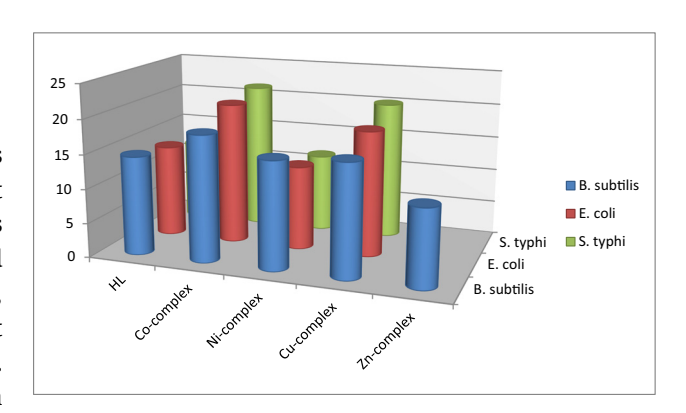


Figure 2: In vitro antibacterial activity of the ligand and its mixedligand complexes.

Table 3: The list of intermolecular interactions between the compounds docked with 426S

Co-crystallized -21.63 0.04 LEU 417, LEU 389, LYS 413, LEU 414, LEU 411, ASN 410, TYR 409, PHE 385 Schiff base ligand -41.40 0.05 LEU 417, LEU 389, LEU 414, LYS 413, PHE 385, LEU 411, ASN 410, TYR 409, CYS 383, GLU 382, ASN 408, LYS 587 [Nil, L, C, L] 2 L, C 2 L,	Hydrogen bond	Bond length (Å)
-41.40 0.05 1 -26.64 0.04 1 -26.10 0.02 1 -25.85 0.04 9	3, LEU 414, LEU 411, ASN 410, TYR 409, N sp ² (N2)–0 sp ² -GLU 382 32, CYS 383, ASP 384, SER 386, PHE 385 O sp ³ (01)–N sp ² -PHE 385	3.078
-41.40 0.05 1 -26.64 0.04 1 -26.10 0.02 1 -25.85 0.04 5		3.043
-41.40 0.05 1 -26.64 0.04 1 -26.10 0.02 1 -25.85 0.04 9	0 sp ³ (03)-0 sp ² -GLU 382	2.866
-41.40 0.05 1 -26.64 0.04 1 -25.85 0.04 1 1 1 1 1 1 1 1 1	$0 \text{ sp}^3(03) - \text{N sp}^3 - \text{LYS } 413$	3.333
-41.40 0.05 1 -26.64 0.04 1 -26.10 0.02 1 -25.85 0.04 1 1 -25.85 0.04 1 1 1 1 1 1 1 1 1	$0 \text{ sp}^3(04) - \text{N sp}^3 - \text{LYS } 413$	3.082
-26.64 0.04 L -26.10 0.02 L -25.85 0.04 S	4, LYS 413, PHE 385, LEU 411, ASN 410, $O \text{ sp}^3(00)$ -O sp^2 -GLU 382	3.077
-26.64 0.04 L -26.10 0.02 L -25.85 0.04 S	82, ASN 408, LYS 587 N sp ³ (N10)-O sp ² -GLU 382	3.018
-26.64 0.04 L -26.10 0.02 L -25.85 0.04 S	$N sp^{3}(N10)-N sp^{3}-LYS 413$	3.155
-26.64 0.04 L -26.10 0.02 L -25.85 0.04 S	$N sp^{2}(N13)-0 sp^{2}-GLU 382$	2.696
-26.64 0.04 1 1 -26.10 0.02 1 1 -25.85 0.04 5 1 1 1 1 1 1 1 1 1 1 1 1 1 1 1 1 1 1	$N sp^{2}(N11)-N sp^{3}-LYS 413$	3.084
-26.64 0.04 1 -26.10 0.02 1 -25.85 0.04 2 3 86 0.08 1 1	$N sp^{2}(N11)-N sp^{2}-ASN 410$	2.849
-26.10 0.02 L -25.85 0.04 S	3, LEU 414, LEU 389, SER 386, ASN 410, $O sp^3(013)$ -N sp^3 -LYS 413	3.140
-26.10 0.02 L -25.85 0.04 S	9, GLU 382, PHE 385, ASP 384, CYS 383	
25.85 0.04 5 5 5 5 5 5 5 5 5 5 5 5 5 5 5 5 5 5 5	3, LEU 414, LEU 389, SER 386, ASN 410, O sp ³ (O13)-N sp ³ -LYS 413	3.156
-25.85 0.04 5 -25.85 0.04 5	9, GLU 382, PHE 385, ASP 384, CYS 383	
T 800 98 86	2, LEU 411, ASN 410, ALA 434, SER 435, O $sp^3(013)$ -N sp^3 -ASN 410	3.044
73.86 0.08	98	
00:0	EU 417, SER 416, LYS 413, LEU 414, LEU 389, SER 386, ASN 410, 0 sp³(013)–N sp³-LYS 413	3.014
LYS 587, LEU 411, TYR 409, GLU 382, PHE 385, ASP 384, CYS 383	9, GLU 382, PHE 385, ASP 384, CYS 383	

*The docking score (PLANTS_{PLP} score) is a function described in Korb et al. [31]. **The numbering of the atoms was done according to the software (Figures 1 and 2).

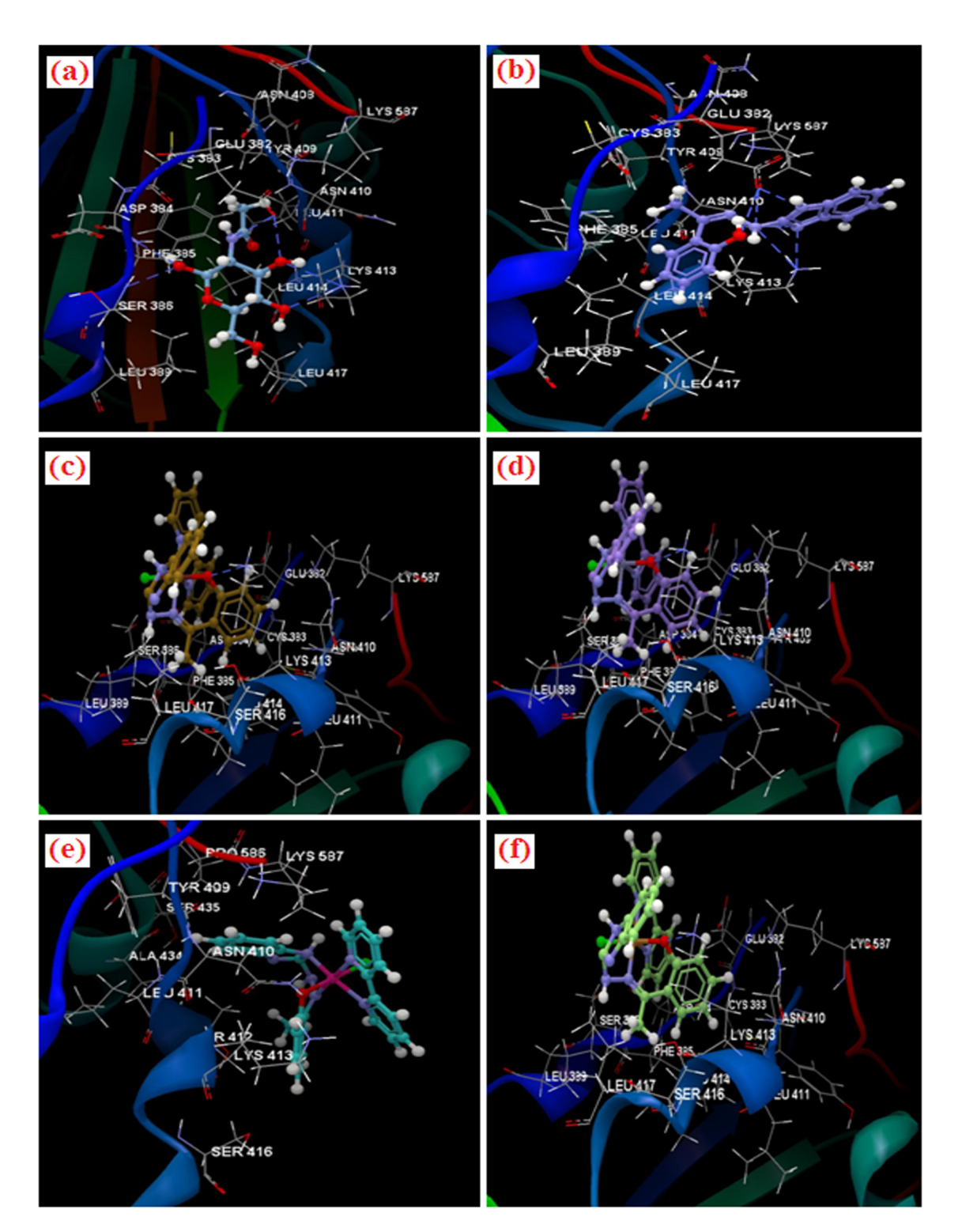


Figure 3: Docking pose of the compounds interacting with the residues of amino acid of binding site of 4Z6S; (a) co-crystallized NAG, (b) Schiff base ligand, (c) Ni(II) complex, (d) Zn(II) complex, (e) Co(II) complex and (f) Cu(II) complex.

the compounds were docked on the crystal structure of MERS CoV (PDB ID: 4Z6S). The docking pose of the co-crystallized N-acetyl-D-glucosamine (NAG) interacting with the residues of amino acid of active site are listed in

Figure 3. The co-crystallized NAG displayed the occurrence of six hydrogen bonds: two with GLU 382 (3.078 and 2.866 Å), two with LYS 413 (3.333 and 3.082 Å), PHE 385 (3.016 Å) and SER 386 (3.043 Å). The co-crystallized

Table 4: The list of intermolecular interactions between the compounds docked with 6W63

Ligand Score*		ISD (Å)	RMSD (\AA) Group interaction	Hydrogen bond**	Bond length (\mathring{A})
Co-crystallized –56.	-56.57 1.53	53	THR 190, GLN189, VAL 186, ARG 188, MET 49, TYR 54, ASP 187, PRO 168, LEU 167,	0 sp ² (001)–N sp ² -GLY 143	3.202
			GLU 166, MEI 165,HIS 164, HIS 1/2, HIS 163, CYS 145, ASN 142, GLY 143, SEK 144, LEU 141, PHE 140, GLY 143, LEU 127, THR 26, THR 25, VAL 42, HIS 41, CYS 44	U sp* (U13)–N sp*-GLU 166	2./21
Schiff base -49.9	-49.91 0.87	13	ALA 191, VAL 186, GLN 192, THR 190, GLN 189, ARG 188, ASP 187, HIS 41, LEU 50,	$0 \text{ sp}^3(00) - \text{N sp}^2 - \text{GLN } 192$	3.028
ligand			PRO 52, ASP 48, CYS 44, TYR 54, MET 49, PRO 168, LEU 167, GLU 166, MET 165	$0 \text{ sp}^3(00) - 0 \text{ sp}^2$ -THR 190	2.558
				$0 \text{ sp}^3(00)$ -N sp ² -THR 190	2.924
				$0 \text{ sp}^3(00) - 0 \text{ sp}^2 - \text{ARG } 188$	3.025
$[CoL_1L_2CI]2H_2O$ -52.52	52 0.002	102	ALA 191, GLN 192, THR 190, GLN 189, ARG 188, ASP 187, MET 49, THR 169, PRO 168,	$N sp^{3}(N23)-N sp^{2}-GLN 189$	3.143
			LEU 167, GLY 170, GLU 166, MET 165, HIS 164, HIS 163, CYS 145, ASN 142		
$[NiL_1L_2CI]2H_2O$ -52.35	35 0.006	900	ALA 191, GLN 192, THR 190, GLN 189, ARG 188, ASP 187, MET 49, THR 169, PRO 168,	$N sp^3(N23)-N sp^2-GLN 189$	3.145
			LEU 167, GLY 170, GLU 166, MET 165, HIS 164, HIS 163, CYS 145, ASN 142		
[ZnL ₁ L ₂ Cl]2H ₂ O -52.23	23 0.01	11	ALA 191, GLN 192, THR 190, GLN 189, ARG 188, ASP 187, MET 49, THR 169, PRO 168,	$N sp^3(N23)-N sp^2-GLN 189$	3.136
			LEU 167, GLY 170, GLU 166, MET 165, HIS 164, HIS 163, CYS 145, ASN 142		
$[CuL_1L_2Cl]2H_20$ –51.9	-51.97 0.01	11	ALA 191, GLN 192, THR 190, GLN 189, ARG 188, ASP 187, MET 49, HIS 41, VAL 186, THR 169,	$N sp^3(N23)-N sp^2-GLN 189$	3.134
			PRO 168, LEU 167, GLY 170, GLU 166, MET 165, HIS 164, HIS 163, CYS 145, ASN 142		

The docking score (PLANTS_{PLP} score) is a function described in Korb et al. [31]. ** The numbering of the atoms was done according to the software (Figures 1 and 2).

NAG was considered as the reference ligand to compare the docking results of the studied compounds. The docking studies revealed that the docking score of all the metal complexes are greater than the co-crystallized NAG (docking score: -21.63; root-mean-square deviation [RMSD]: 0.04 Å) but smaller than L_1 (docking score: -41.40; RMSD: 0.05 Å; Table 4). The L₁ showed the presence of six hydrogen bonds: three with GLU 382 (3.077, 3.018 and 2.696 Å), two with LYS 413 (3.155 and 3.084 Å) and one with ASN 410 (2.849 Å). The Ni(II) complex with the best docking score (-26.64; RMSD: 0.04) displayed one hydrogen bond with LYS 413 (3.140 Å). With LYS 413 amino acid, Zn(II) complex (3.156 Å) and Cu(II) complex (3.014 Å) realized one more hydrogen bond. However, Co(II) complex realized one hydrogen bond with ASN 410 (3.044 Å). The docking pose of the compounds interacting with amino acid residues is presented in Figure 3. The amino acid residues that formed the interacting group of each compound are listed in Table 3. After analyzing the data, it was noticed that all the studied compounds were placed in the same binding site (represented by a green sphere) of 4ZS6 as the co-crystallized one and have the same orientation as the co-crystallized NAG (Figure 4).

3.4.2 Docking evaluation against SARS-CoV-2 Mpro

All the compounds were docked on the crystal structure of SARS-CoV-2 M^{pro} (PDB ID: 6W63). The docking pose of the co-crystallized X77 interacting with amino acid residues of the active site and the hydrogen bonds created with GLU 166 (2.721 Å) and GLY 143(3.202 Å) is shown in Figure 5. The co-crystallized X77 (N-(4-tert-butylphenyl)-N-[(1R)-2-(cyclohexylamino)-2-oxo-1-(pyridin-3-yl)ethyl]-1H-imidazole-4-carboxamide) was considered as a standard ligand to compare the docking results of the studied compounds. The docking studies revealed that the docking

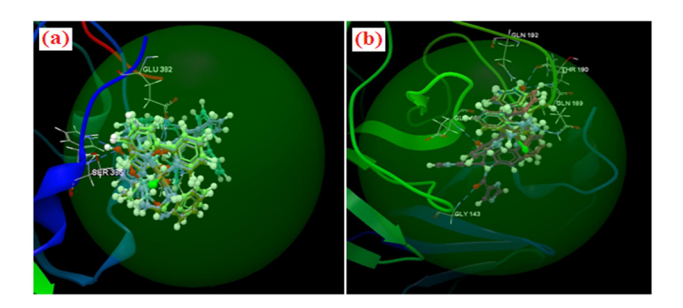


Figure 4: (a) Docking pose of the co-crystallized NAG and all compounds in the binding site of 4Z6S and (b) docking pose of the co-crystallized X77 and all compounds in the binding site of 6W63.

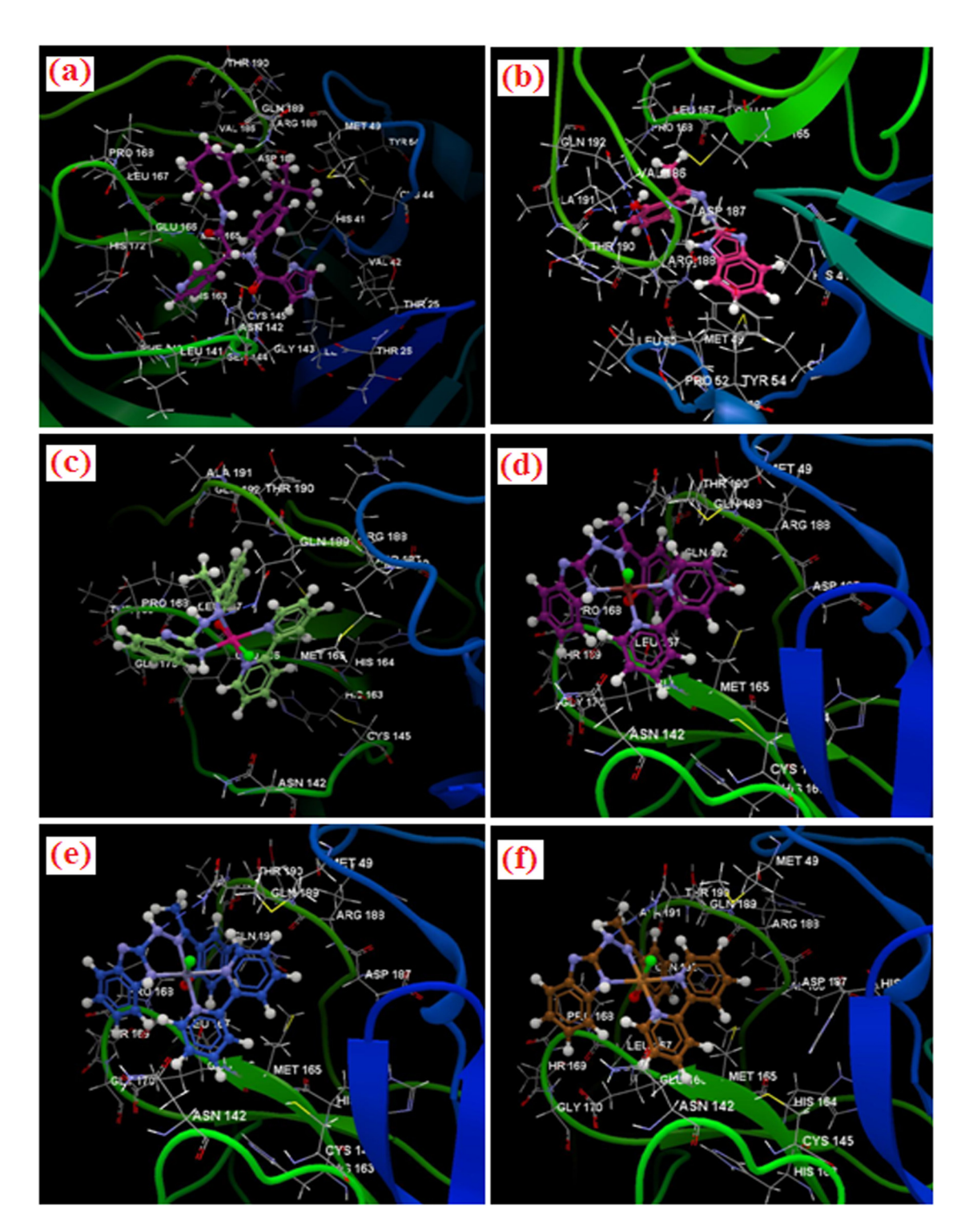


Figure 5: Docking pose of the compounds interacting with the amino acid residues of binding site of 4Z6S; (a) co-crystallized X77, (b) Schiff base ligand, HL, (c) Co(II) complex, (d) Ni(II) complex, (e) Zn(II) complex and (f) Cu(II) complex.

score of all the metal complexes are close to that of the co-crystallized X77 (docking score: -56.57; RMSD: 1.53 Å) and greater than the Schiff base ligand, L_1 (docking score: -49.91; RMSD: 0.87 Å; Table 5). The Schiff base ligand, L₁,

showed the occurrence of four hydrogen bonds: one with GLN 192 (3.028 Å), two with THR 190 (2.558 and 2.924 Å) and one with ARG 188 (3.025 Å). The Co(II) complex with the best docking score (-52.52; RMSD: 0.002) displayed

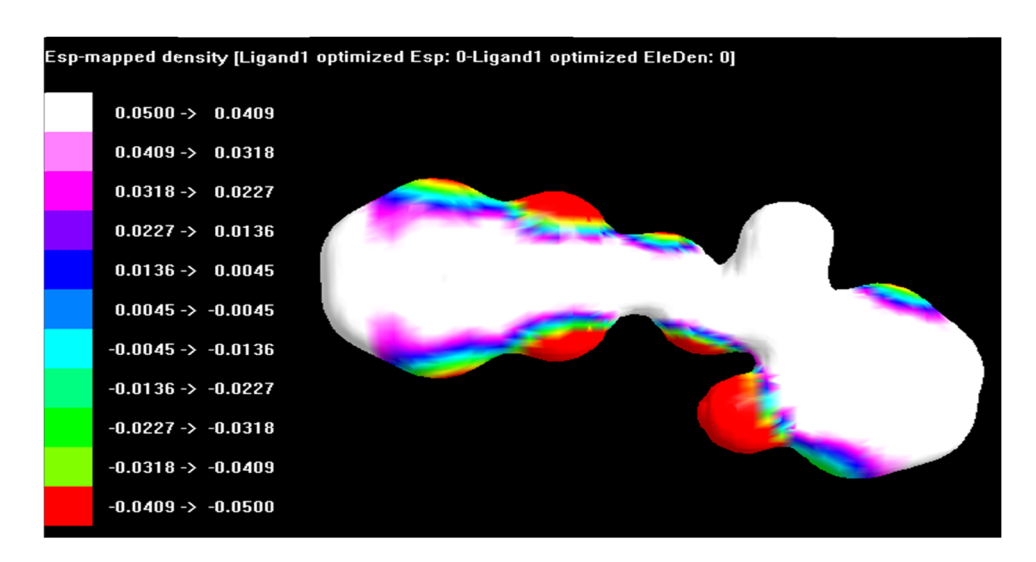


Figure 6: The ESP surface of the Schiff base ligand, L1.

one hydrogen bond with GLN 189 (3.143 Å). With the GLN189 amino acid, Ni(II) complex (3.145 Å), Zn(II) complex (3.145 Å) and Cu(II) complex (3.134 Å) realized one more hydrogen bond. The docking pose of the compounds interacting with amino acid residues is presented in Figure 5. The amino acid residues that formed the interacting group of each compound are listed in Table 4. After analyzing the data, it was noticed that the all studied compounds were placed in the same binding site (represented by a green sphere) of 6W63 as the cocrystallized one and have the same orientation as the cocrystallized X77 (Figure 5).

According to Lipinski's rule of five, the calculated parameters (Table S2) may predict the property of a molecule to turn into an active drug [48] on the basis of the number of violations made. It is observed that all metal complexes have two violations of Lipinski's rule of five (Lipinski violation is 2), namely, molecular weight >500 Da and octanol-water partition coefficient ($\log P$) >5.

3.5 Electrostatic potential (ESP) surface analysis

The ESP surface of Schiff base ligand, L_1 , was analyzed by using Argus Lab 4.0.1 software as shown in Figure 6. The surface contains a number of possible sites for electrophilic attack. The ESP surface displayed a specific data about the charge distribution. The negative regions were mainly over phenolic oxygen, azomethine nitrogen and benzimidazole ring nitrogen atoms as indicated in red and were involved in coordination. However, the other

nitrogen atom was not involved in coordination likely due to the steric effect.

4 Conclusion

A series of mixed-ligand complexes with Cu(II), Co(II), Ni(II) and Zn(II) ions were investigated. The antibacterial activity suggested the moderate antibacterial activity for all the complexes in comparison to the Schiff base ligand. However, the Zn(II) complex was inactive against E. coli and S. typhi. Moreover, molecular docking studies recorded against MERS-CoV (PDB ID: 4ZS6) and SARS-CoV-2 M^{pro} (PDB ID: 6W63) revealed that all the studied metal complexes demonstrated two violations of all the parameters involved in the Lipinski's rule of five. The Ni(II) complex displayed the best docking score (-26.64; RMSD: 0.04) against MERS-CoV whereas the Co(II) complex displayed the best docking score (-52.52; RMSD: 0.002) against SARS-CoV-2 M^{pro}. This study may be helpful for the researchers in designing new potent drugs. In addition, the ESP surface of the Schiff base ligand, L₁, was analyzed to understand the possible sites for electrophilic attack.

Acknowledgments: The authors acknowledge the financial support through Researchers Supporting Project number (RSP-2020/147), King Saud University, Riyadh, Saudi Arabia. The authors are highly thankful to Dr. Lucia Pintilie for her valuable support in the docking analyses.

Research funding: The authors acknowledge the financial support through Researchers Supporting Project number (RSP-2020/147), King Saud University, Riyadh, Saudi Arabia.

Author contribution: Ranjan K. Mohapatra designed and supervised the study. V. P. Saikishore performed the study. Susanta K. Biswal supervised and was in charge of the initial draft. Mohammad Azam was involved in final editing and also revised the manuscript.

Conflict of interest: There are no conflicts to declare.

Data availability statement: All data presented in the study are included in the article and supplementary material.

References

- Devinder MRJ, Michael BR, Sean MK. Synthesis and evaluation of anticancer benzoxazoles and benzimidazoles related to UK-1. Bioorg Med Chem. 2002;10:3997-4004.
- Hong SY, Chung KH, You JH, Choi IH, Chae MJ, Han JY, et al. Synthesis and biological evaluation of benzimidazole-4,7diones that inhibit vascular smooth muscle cell proliferation. Bioorg Med Chem Lett. 2004;14:3563-6.
- Lopez VF, Medina-Franco JL, Hernandez-Campos A, Rodriguez-Morales S, Yepez L, et al. Molecular modeling of some 1Hbenzimidazole derivatives with biological activity against Entamoebahistolytica: a comparative molecular field analysis study. Bioorg Med Chem. 2007;15:1117-26.
- Chkirate K, Karrouchi K, Dege N, Sebbar NK, Ejjoummany A, Radi S, et al. Co(II) and Zn(II) pyrazolyl-benzimidazole complexes with remarkable antibacterial activity. New J Chem. 2020:44:2210-21.
- White AW, Curtin NJ, Eastman BW, Golding BT, Hostomsky Z, Kyle S, et al. Potentiation of cytotoxic drug activity in human tumour cell lines, by amine substituted 2-arylbenzimidazole-4-carboxamide PARP-1 inhibitors. Bioorg Med Chem Lett. 2004;14:2433-7.
- Driessen WL, Wiesmeijer WGR, Schipper-Zablotskaja M, De Graaff RAG, Reedijk J. Transition metal coordination compounds of two pyrazole-substituted ammonia ligands. X-ray structure of [bis(1-pyrazolylmethyl)aminecobalt(II)] bis (nitrate). Inorg Chim Acta. 1989;162:233-8.
- Boca M, Jameson RF, Linert W. Fascinating variability in the chemistry and properties of 2,6-bis-(benzimidazol-2-yl)pyridine and 2,6-bis-(benzthiazol-2-yl)-pyridine and their complexes. Coord Chem Rev. 2011;255:290-317.
- Bouchouit M, Said ME, Kara Ali M, Bouacida S, Merazig H, KacemChaouche H, et al. Synthesis, X-ray structure, theoretical investigation, corrosion inhibition and antimicrobial activity of benzimidazole thioether and theirs metal complexes. Polyhedron. 2016;119:248-59.

- Gocke M, Utku S, Gur S, Ozkul A, Gumus F. Synthesis, in vitro cytotoxic and antiviral activity of cis-[Pt(R(-) and S(+)-2- α hydroxybenzylbenzimidazole)Cl] complexes. Eur J Med Chem. 2005;40:135-41.
- Saczewski F, Dziemidowicz-Borys E, Bednarski PJ, Grünert R, Gdaniec M, Tabin P. Synthesis, crystal structure and biological activities of copper(II) complexes with chelating bidentate 2-substituted benzimidazole ligands. J Inorg Biochem. 2006;100:1389-98.
- Khan SA, Noor A, Kempe R, Subhan H, Shah A, Khan E. [11] Syntheses, molecular structure, and electrochemical investigations of cobalt(II), copper(II), palladium(II), and zinc(II) complexes with 3-methylpyrazole. J Coord Chem. 2014:67:2425-34.
- [12] Khan E, Khan SA, Zahoor M, Tahir MN, Noor A, Altaf AA. Cu(II) coordination polymers stabilized by pyridine-2,6-dicarboxylate anion and pyrazole derivatives through ligand hydrolysis. J Coord Chem. 2018;71:2658-73.
- [13] Alvareza N, Mendesb LFS, Kramerc MG, Torrea MH, Costa-Filhob AJ, Ellenad J, et al. Development of copper(II)-diimineiminodiacetate mixed ligand complexes as potential antitumor agents. Inorg Chim Acta. 2018;483:61-70.
- Albobaledia Z, Esfahania MH, Behzada M, Abbasi A. Mixed ligand Cu(II) complexes of an unsymmetrical Schiff base ligand and N-donor heterocyclic co-ligands: Investigation of the effect of co-ligand on the antibacterial properties. Inorg Chim Acta. 2020;499:119185.
- Eremina JA, Lidera EV, Samsonenko DG, Sheludyakova LA, [15] Berezina AS, Klyushova LS, et al. Mixed-ligand copper(II) complexes with tetrazole derivatives and 2,2'-bipyridine, 1,10phenanthroline: Synthesis, structure and cytotoxic activity. Inorg Chim Acta. 2019;487:138-44.
- Bianchia A, Delgado-Pinar E, García-España E, Giorgia C, Pina F. Highlights of metal ion-based photochemical switches. Coord Chem Rev. 2014;260:156-215.
- [17] Costa RD, Orti E, Bolink HJ, Monti F, Accorsi G, Armaroli N. Luminescent ionic transition-metal complexes for lightemitting electrochemical cells. Angew Chem Int Ed. 2012;51:8178-211.
- [18] Katari M, Carmichael D, Jacquemin D, Frison G. Structure of electronically reduced N-donor bidentate ligands and their heteroleptic four-coordinate zinc complexes: a survey of density functional theory results. Inorg Chem. 2019;58:7169-79.
- [19] Lu J, Guo J, Sang W, Guo H. Mixed-ligand oxovanadium complexes incorporating Schiff base ligands: synthesis, DNA interactions, and cytotoxicities. Trans Met Chem. 2013;38:481-8.
- [20] Sigel H, Sigel A. Metal ions in biological systems. Vols. 12 and 13. New York: Marcel Dekker; 2005.
- Mohapatra RK, Pintilie L, Kandi V, Sarangi AK, Das D, Sahu R, Perekhoda L. The recent challenges of highly contagious COVID-19 causing respiratory infections: symptoms, diagnosis, transmission, possible vaccines, animal models and immunotherapy. Chem Biol Drug Des. 2020;96:1187-120.
- [22] Mohapatra RK, Rahman M. Is it possible to control the outbreak of COVID-19 in Dharavi, Asia's largest slum situated in Mumbai? Anti-Infective Agents. 2020. doi: 10.2174/ 2211352518999200831142851.

- [23] Mohapatra RK, Das PK, Kandi V. Challenges in controlling COVID-19 in migrants in Odisha, India, diabetes & metabolic syndrome. Clin Res Rev. 2020;14:1593-4.
- [24] Ancy I, Sivanandam M, Kumaradhas P. Possibility of HIV-1 protease inhibitors-clinical trial drugs as repurposed drugs for SARS-CoV-2 main protease: a molecular docking, molecular dynamics and binding free energy simulation study. J Biomol Struct Dyn. 2020. doi: 10.1080/ 07391102.2020.1786459
- [25] Sang P, Tian S-H, Meng Z-H, Yang L-Q. Anti-HIV drug repurposing against SARS-CoV-2. RSC Adv. 2020;10:15775-83.
- [26] Cardoso WB, Mendanha SA. Molecular dynamics simulation of docking structures of SARS-CoV-2 main protease and HIV protease inhibitors. J Mol Struct. 2021;1225:129143.
- [27] Mohapatra RK, Das PK, El-ajaily MM, Mishra U, Dash DC. Synthesis, spectral, thermal, kinetic and antibacterial studies of transition metal complexes with benzimidazolyl-2hydrazones of o-hydroxyacetophenone, o-hydroxybenzophenone and o-vanillin. Bull Chem Soc Ethiop. 2018;32(3):437-50.
- [28] CLC Drug Discovery Workbench, available from http://www. clcbio.com.
- [29] Yu X, Zhang S, Jiang L, Cui Y, Li D, Wang D, et al. Structural basis for the neutralization of MERS-CoV by a human monoclonal antibody MERS-27. Sci Rep. 2015;5:13133. doi: 10.1038/ srep13133
- [30] Mesecar AD. A taxonomically-driven approach to development of potent, broad-spectrum inhibitors of coronavirus main protease including SARS-CoV-2 (COVID-19); 2020. https:// www.rcsb.org/structure/6W63.
- [31] Korb O, Stützle T, Exner TE. Empirical scoring functions for advanced protein-ligand docking with plants. J Chem Inf Model. 2009;49:84-96.
- [32] Azam M, AlResayes SI. Phenoxy-bridged binuclear Zn(II) complex holding salen ligand: synthesis and structural characterization. Mol Structure. 2016;1107:77-81.
- [33] Nakamoto K. Infrared and Raman spectra of inorganic and coordination compounds. New York: Wiley; 1986.
- [34] Azam M, Dwivedi S, AlResayesSI, Adil SF, Islam MS, Kruszynska AT, Kruszynski R, Lee DU. Cu(II) salen complex with propylene linkage: An efficient catalyst in the formation of C-X bonds (X = N, O, S) and biological investigations. J Mol Struct. 2017;1130:122-7.
- [35] Azam M, Khan AA, AlResayes SI, Islam MS, Saxena AK, Dwivedi S, Musarrat J, Kruszynska AT, Kruszynski R. Synthesis and characterization of 2-substituted benzimidazoles and their evaluation as anticancer agent. Spectrochim Acta Part A. 2015;142:286-91.
- [36] Azam M, AlResayes SI, Kruszynska AT, Kruszynski R, Verma A, Pati UK. Chiral anionic binuclear zinc complexes based on diaminocyclohexane ligand and their in vitro antiproliferative studies. Inorg Chem Commun. 2014;46:73-80.

- [37] Abd El-halim HF, Omar MM, Mohamed GG. Synthesis, structural, thermal studies and biological activity of a tridentate Schiff base ligand and their transition metal complexes. Spectrochim Acta Part A. 2011;78:36-44.
- [38] Firdaus F, Fatma K, Azam M, Khan SN, Khan AU, Shakir M. Template synthesis and physico-chemical studies of 14membered hexamacrocyclic complexes with Co(II), Ni(II), Cu (II) and Zn(II): a comparative spectroscopic approach on DNA binding with Cu(II) and Ni(II) complexes. Trans Met Chem. 2008;33:467-73.
- [39] Lever ABP. Inorganic electronic spectroscopy. 2rd edn. Amsterdam: Elsevier; 1984.
- [40] Firdaus F, Fatma K, Azam M, Khan SN, Khan AU, Shakir M. Template synthesis and physic-chemical characterization of 14-membered tetraiminemacrocyclic complexes, $[MLX_2]$ [M = Co(II), Ni(II), Cu(II) and Zn(II)]: DNA binding study on [CoLCl₂] complex. Spectrochim Acta Part A. 2009;72:591-6.
- [41] Shakir M, Azam M, Naseem S, Khan AU. Template synthesis and physic-chemical studies of 14-membered functionalized Pendant arm Schiff base macrocyclic complexes of Co(II), Ni(II), Cu(II) and Zn(II): DNA binding studies on Cu(II). Synth React Inorg-Metal Org Nano-Met Chem. 2011;41:1056-62.
- [42] Shakir M, Azam M, Parveen S, Khan AU, Firdaus F. Synthesis and spectroscopic studies on complexes of N,N-bis(-(2-pyridenecarboxaldimine)-1,8-diaminonaphthalene (L): DNA binding studies on Cu(II) complex. Spectrochim Acta Part A. 2009;71:1851-6.
- [43] Shakir M, Azam M, Azim Y, Parveen S, Khan AU. Synthesis and physico-chemical studies on complexes of 1,2-diaminophenyl-N,N'-bis(2-pyridenecarboxaldimine) (L): a spectroscopic approach on DNA binding studies on Cu(II) complex. Polyhedron. 2007;26:5513-5518.
- [44] Cotton FA, Wilkinson G. Advanced inorganic chemistry. 5th edn. New York: Wiley; 1988.
- [45] Shakir M, Abbasi A, Azam M, Khan AU. Synthesis, spectroscopic studies and crystal structure of the Schiff base ligand L derived from condensation of 2-thiophenecarboxaldehyde and 3,3' diaminobenzi-dine and complexes with Co(II), Ni(II), Cu (II), Cd(II) and Hg(II). Comparative DNA binding studies of L and its Co(II), Ni(II) and Cu(II) complexes. Spectrochim Acta Part A. 2011;79:1866-75.
- [46] Balhausen CJ. An introduction to ligand field. New York: McGraw Hill; 1962.
- [47] El-Gamel NEA. Metal chelates of ampicillin versus amoxicillin: synthesis, structural investigation, and biological studies. J Coord Chem. 2010;63:534-43.
- [48] Lipinski CA, Lombardo F, Dominy BW, Feeney PJ. Experimental and computational approaches to estimate solubility and permeability in drug discovery and development settings. Adv Drug Delivery Rev. 2001;46:3-26.